Impact of applied strain on the electron transport through ferroelectric tunnel junctions

Xin Luo, S. P. Lin, Biao Wang, and Yue Zheng

Citation: Appl. Phys. Lett. **97**, 012905 (2010); doi: 10.1063/1.3462070
View online: http://dx.doi.org/10.1063/1.3462070
View Table of Contents: http://aip.scitation.org/toc/apl/97/1
Published by the American Institute of Physics

Impact of applied strain on the electron transport through ferroelectric tunnel junctions

Xin Luo, S. P. Lin, Biao Wang,[a] and Yue Zheng[a]
State and Key Laboratory of Optoelectronic Materials and Technologies, Institute of Optoelectronic and Functional Composite Materials, and School of Physics and Engineering, Sun Yat-sen University, 510275 Guangzhou, People's Republic of China

(Received 19 April 2010; accepted 16 June 2010; published online 9 July 2010)

Combining nonequilibrium Green's functions with density-functional theory, we have investigated the effect of external strain field on the tunneling electroresistance (TER) of ferroelectric material sandwiched between Pt electrodes. The results show that the strain induced para/ferroelectric phase transitions play an important role in the electronic transport properties of the junction. Sizable enhancements in the resistance are found for the strained ferroelectric junctions with a TER ratio of 9000%. Detail analyses show that the Ti–O displacements along the transport direction in ferroelectric barrier change the effective potential profile, resulting in a giant piezoelectric resistance in the ferroelectric tunnel junctions. © *2010 American Institute of Physics*. [doi:10.1063/1.3462070]

Ferroelectric (FE) thin films have aroused great interest in recent years for its diverse functionality in devices such as the actuator, sensors, and nonvolatile FE memories. In particular, the perovskite FE material is promising due to its potential application in the FE tunnel junctions (FTJs).[1–3] Unlike the common magnetic tunnel junctions constructed with MgO as the barrier, FTJ use FEs as tunneling barriers. Since the FE is a collective effect, it was thought for a long time that it will be suppressed in small particles or thin films below a critical thickness.[4] With improvement in the fabrication and characterization techniques, recent experiments have demonstrated that the FE can persist in the nanometer scale FE thin film.[5,6] These discoveries renew the FE thin film to a high level of excitement and huge researches are devoted to the development of FTJ (Refs. 7 and 8) and the related large density nonvolatile FE random access memories (FERAMs).[9,10]

When the thickness of FE film approaches several nanometers, the tunneling leakage current becomes the dominant source of conduction. The underlying principles of FTJ employ the physics of spontaneous polarization dependent tunneling in FE barriers. Experimental and theoretical works indicated that the tunneling electroresistance (TER) across FE barriers can vary significantly in asymmetry FTJ when the polarization is reversed.[3,11] Up to now, great efforts have been devoted to the effect of ferroelectricity and magnetization on electron transport in FTJ.[12,13] Since the performance of FTJ based devices depends on the response of FEs to external perturbations, and the properties of FE barriers are sensitive to the applied mechanical loads.[11,14] In the pioneering paper of FTJ,[2] the influence of converse piezoelectric effect on the tunnel current is described in a one-band model, which predicted a strain-related resistive switching. Given the importance of strains effect on the polarization and electroresistance in nanoscale FTJ, we combine more precise nonequilibrium Green's function technique with density functional theory (DFT) to calculate the electronic transport properties of FTJ and provide a physical analysis of the strain dependent giant TER.

In the present work, we constructed a model of $Pt_5/TiO_2-(PbTiO_3)_4/Pt_4$ multilayer to explore the significant role of external applied strain on the electronic transport properties of FTJ. The atomic structural relaxation and the electronic states were performed using the Vienna *Ab initio* Simulation Package (VASP) (Ref. 15) employing the projector augmented wave[16] method within the local density approximation (LDA).[17] The TiO_2 terminated interface with O atoms located on top of the outmost Pt electrode layer was chosen in our model for its relatively strong cohesive energy. We first consider the structure evolution of the $Pt/PbTiO_3/Pt$ junction with respect to a wide range of applied strain $\eta=(a_s-a_0)/a_s$,[18] where a_s is the in-plane lattice constant of strained junction and a_0 is the relaxed lattice constant of free $PbTiO_3$. The strain field can be induced by the applied stress, and the atomic positions are relaxed the along the interface normal direction with the constants that the in-plane lattice constants are fixed to a_s.

By comparing the lowest energy of the relaxed junctions with paraelectric (PE) and FE state barriers, it is found that the four unit cells $PbTiO_3$ tunneling barrier tend to be in PE state due to the incomplete screening of the depolarization field. Interestingly, the PE state barriers become less stable with increasing compressive strain, and switch to FE state when the external applied strain reaches the critical value of -1.12%. Thus, we can use the applied strain to tune the critical thickness, below which the ferroelectricity disappears. Figure 1 shows the central part of the relaxed $Pt/PbTiO_3/Pt$ FE junctions under two different mechanical loads. Without the external strain, the atomic displacements are symmetry in the barrier [Fig. 1(a)] with two dipoles pointing toward the barrier at both Pt/TiO_2 interface. With an applied compressive strain higher than -1.12%, i.e., -2.57%, there are net shifted displacements of the Ti ions with respect to the center of its O cage in the FE barrier. As a result, the polarization is induced by the holistic dipole orientation, as shown in Fig. 1(b). Moreover, the corresponding real space effective potentials along the transport direction are also given in the background of Fig. 1, where the

[a]Authors to whom correspondence should be addressed. Electronic addresses: wangbiao@mail.sysu.edu.cn and zhengy35@mail.sysu.edu.cn.

 © 2010 American Institute of Physics

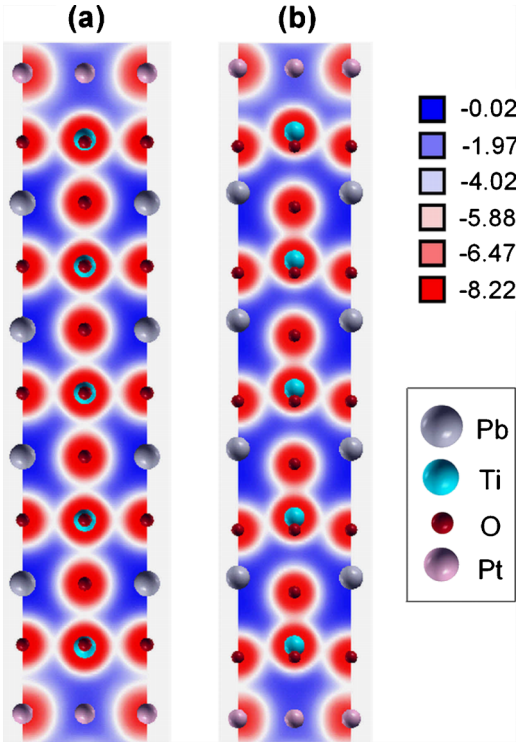

FIG. 1. (Color online) Schematic illustration of the $Pt/PbTiO_3/Pt$ tunneling junction with the FE barrier in (a) unstrained PE state and (b) strain induced FE state. The effective potential profiles are also given in the background; only the central parts of the junctions are shown.

symmetry PE state barrier has a relatively low potential path between the top and bottom electrodes. Increasing the compressive strain leads to large Ti–O displacements in the adjacent unit cells, producing higher potential barrier.

Since the major interest of the FTJ is in its TER under different external perturbations, we used the ATOMISTIX TOOLKIT package (ATK 2008.10),[19] which combines nonequilibrium Green's function technique with the self-consistent pseudopotential method in the framework of DFT, to explore the electron transport properties of FTJ under different applied strains.[20] The calculated transmission spectra for the highly strained FE state junction and unstrained PE state junction are given in Fig. 2. Indeed, the transmission spectra differ from each other, suggesting the changes of electron states in the two different strained junctions. The overall transmission of the unstrained PE junction is higher than that of the strained FE junction, especially for the energy window just above the Fermi level. That means the transmission peaks in the unstrained PE state junction will contribute to its conductance under a small voltage bias. According to quantum mechanics,[21] the conductance of above systems can be expressed by the sum of zero voltage transmission probability at the Fermi energy E_F. In our calculation, we find that the conductance of the unstrained PE state junction is $77.3\times10^{-4}\ e^2/h$, however, the corresponding value for the strained FE state junction is $2.8\times10^{-4}\ e^2/h$. These results are in consistent with the $Pt/BaTiO_3/Pt$ FTJ,[12] which obtained a TER ration of 6 during PE/FE phase transition without strains. Within the strain engineering, we can produce a significant larger TER ratio of 28 through the manipulation of the PE/FE transition. To quantify the sensitivity of the TER with the applied mechanical forces, we have defined the giant piezoelectric resistance (GPR)

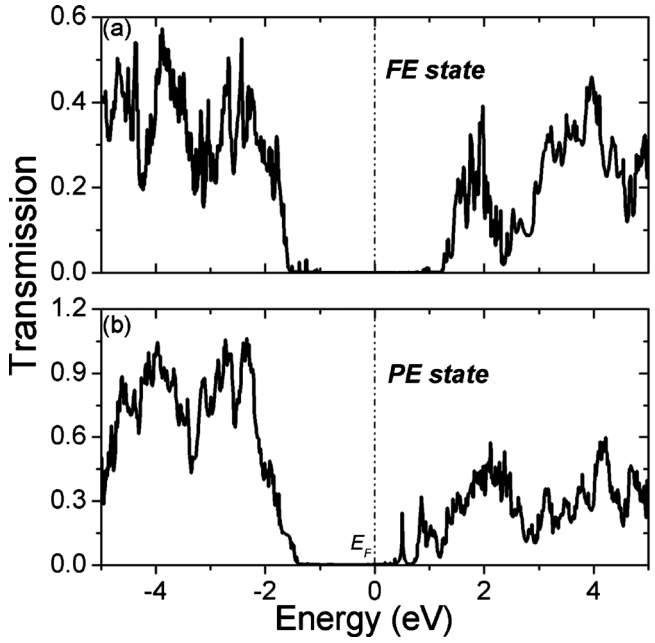

FIG. 2. Dependence of the transmission spectra on the energy for junctions with (a) strain induced FE state barrier and (b) unstrained PE state barrier. The Fermi level is set to zero.

effect. In this paper, we give GPR effect as a function of the applied strain to describe the strain-dependent tunneling resistance effects, i.e., $GPR=[R_{strained}-R_{unstrained}]/\min(R_{strained},R_{unstrained})$.

Given the importance of FTJ in the large density nonvolatile FERAMs, it is interesting to look at the GPR effect at different voltages. We calculated the voltage dependent current for the unstrained PE junction and the $\eta=-2.57\%$ strained FE junction. The tunneling current is calculated with the Landauer–Büttiker formula as follows:[21,22]

$$I=\frac{2e}{h}\int_{-\infty}^{\infty}T(\varepsilon)\{n_F(\varepsilon-\mu_R)-n_F(\varepsilon-\mu_L)\}d\varepsilon, \quad (1)$$

where μ_L and μ_R is the chemical potential of left and right electrodes, respectively, n_F is the Fermi distribution function, and $T(\varepsilon)$ is the transmission probability of electrons passing through the barrier. Figure 3 shows the current as a function of the applied voltage bias for the two different strained junc-

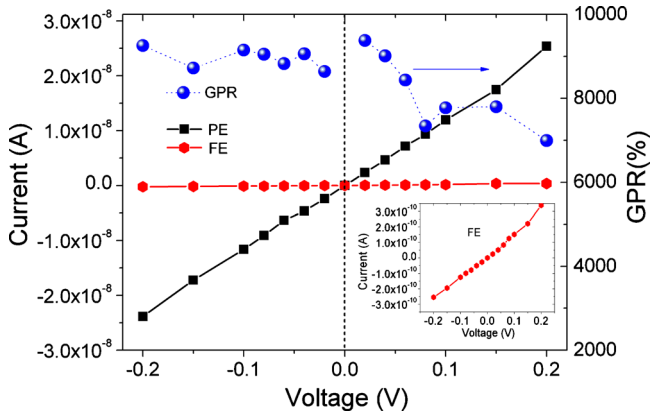

FIG. 3. (Color online) Tunneling current as a function of the applied bias for the PE and FE junctions, and their resistance ratios are depicted by the GPR. The insert shows I-V relationship of the FE junction in a smaller current range.

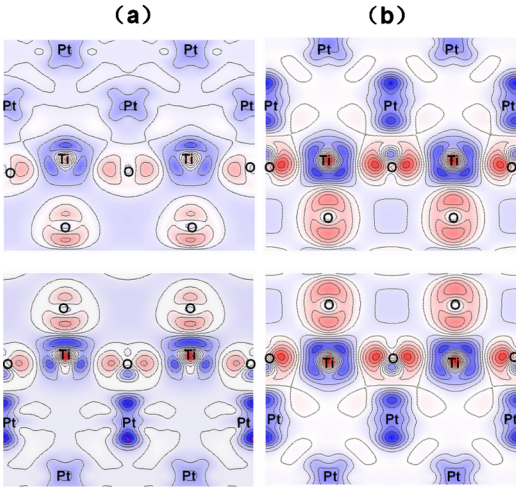

FIG. 4. (Color online) Differential charge density profile for the (a) strain induced FE state junction and (b) unstrained PE state junction.

tions. Indeed, the applied strains have profound effect on the potential barrier of the strained FE junction, and the difference in tunneling current for the two junctions is obvious. In contrast to the low resistance in the unstrained PE junction, the current of the strained FE junction change significantly, with an increase in resistance by about two orders of magnitude. The corresponding GPR ratio can obtain 9000%, which is an important result that has exciting technological implications. It is noted that the I-V curve of the PE junction shows a linear relationship. However, it is not the case in the strained FE junction, which has slightly different slops at the negative and positive bias, as shown in the insert of Fig. 3. As a result, there is 20% variance in the GPR ratio for the forward and the backward bias.

In order to gain more insight into the giant GPR effect and the different slops of I-V curve in the strained FE junction, we plot the differential electron density of the junctions under different applied strains. Figure 4(a) shows the contour plot of induced charge density for the strained FE junction at its two TiO_2/Pt interfaces. The corresponding profiles of the unstrained PE state junction are given in Fig. 4(b). In contrast to the symmetry interface bonding in PE state junction, the microscopic Ti–O dipole displacements of adjacent unit in strained FE junction change the local bonding environment with the electrode. Moreover, the asymmetry deformations of Pt–O bonding redistribute the interfacial charge. Accordingly, the abilities of Pt electrode to screen the polarized charge are different on the top and bottom interfaces. As a result, the Thomas–Fermi screening lengths may be different at both interfaces even with the same Pt electrodes, and the average potential barrier will be varied for the forward and backward bias according to the electrostatic model of Ref. 2. Therefore, the resistances of the strained FE junction are different under positive and negative bias.

In summary, a microscopic physical analysis of the tunneling current in FE junction is performed by using first-principles quantum transport calculations. The electron transport and structural properties of the Pt/$PbTiO_3$/Pt junctions are examined under different applied strain conditions. In particular, a strain induced PE to FE phase transition is predicted in the four unit cell $PbTiO_3$ tunneling junction under -1.12% compressive strains, which demonstrated that the critical thickness can be tuned by applied strain. It is found that the TER changes significantly near this phase transition, with a GPR ratio of about 9000%. The calculations show that the relative Ti–O dipole displacements in the strained FE junction play an important role in the large tunneling resistance. Due to the high-sensitivity to external applied strain, FTJ with the GPR effect should be adequate for applications in agile electronics and other multifunctional devices.

This work was supported by the NSFC (Grant Nos. 10831160504, 10902128, and 10732100) and the Sun Yat-sen Talent Cultured Project (Grant No. 3126201).

[1]E. Y. Tsymbal and H. Kohlstedt, Science **313**, 181 (2006).
[2]H. Kohlstedt, N. A. Pertsev, J. Rodriguez Contreras, and R. Waser, Phys. Rev. B **72**, 125341 (2005).
[3]M. Y. Zhuravlev, R. F. Sabirianov, S. S. Jaswal, and E. Y. Tsymbal, Phys. Rev. Lett. **94**, 246802 (2005).
[4]J. Junquera and P. Ghosez, Nature (London) **422**, 506 (2003).
[5]T. Tybell, C. H. Ahn, and J.-M. Triscone, Appl. Phys. Lett. **75**, 856 (1999).
[6]D. D. Fong, G. B. Stephenson, S. K. Streiffer, J. A. Eastman, O. Auciello, P. H. Fuoss, and C. Thompson, Science **304**, 1650 (2004).
[7]G. Gerra, A. K. Tagantsev, N. Setter, and K. Parlinski, Phys. Rev. Lett. **96**, 107603 (2006).
[8]G. Gerra, A. K. Tagantsev, and N. Setter, Phys. Rev. Lett. **98**, 207601 (2007).
[9]V. Garcia, M. Bibes, L. Bocher, S. Valencia, F. Kronast, A. Crassous, X. Moya, S. Enouz-Vedrenne, A. Gloter, D. Imhoff, C. Deranlot, N. D. Mathur, S. Fusil, K. Bouzehouane, and A. Barthélémy, Science **327**, 1106 (2010).
[10]V. Garcia, S. Fusil, K. Bouzehouane, S. Enouz-Vedrenne, N. D. Mathur, A. Barthélémy, and M. Bibes, Nature (London) **460**, 81 (2009).
[11]Y. Zheng and C. H. Woo, Nanotechnology **20**, 075401 (2009).
[12]J. P. Velev, C. G. Duan, K. D. Belashchenko, S. S. Jaswal, and E. Y. Tsymbal, Phys. Rev. Lett. **98**, 137201 (2007).
[13]J. P. Velev, C. G. Duan, J. D. Burton, A. Smogunov, M. K. Niranjan, E. Tosatti, S. S. Jaswal, and E. Y. Tsymbal, Nano Lett. **9**, 427 (2009).
[14]E. Bousquet, N. Spaldin, and P. Ghosez, Phys. Rev. Lett. **104**, 037601 (2010).
[15]G. Kresse and J. Furthmuller, Comput. Mater. Sci. **6**, 15 (1996).
[16]P. E. Blöchl, Phys. Rev. B **50**, 17953 (1994).
[17]A plane-wave basis set was used for the electron wave function with the cutoff energy of 400 eV. The Brillouin Zone integrations were carried out with a $8\times8\times1$ Monkhorst–Pack k-point mesh together with a 0.2 eV Gaussian broadening. The configuration is considered as relaxed until the maximum Hellman–Feynman force acting on each atom is less than 0.01 eV/Å.
[18]N. A. Pertsev, A. G. Zembilgotov, and A. K. Tagantsev, Phys. Rev. Lett. **80**, 1988 (1998).
[19]M. Brandbyge, J. Mozos, P. Ordejon, J. Taylor, and K. Stokbro, Phys. Rev. B **65**, 165401 (2002).
[20]For the electron transport calculation, the valence electrons are expanded in a numerical atomic-orbital basis set of single zeta plus polarization. A 20×20 k-point mesh is sampled in the surface Brillouin zone for the two-probe system.
[21]S. Datta, *Electronic Transport in Mesoscopic Systems* (Cambridge University Press, Cambridge, 1995).
[22]X. Luo, B. Wang, and Y. Zheng, J. Appl. Phys. **106**, 073711 (2009).